



Dynamic secondary ion mass spectrometry study of surface oxide layers of nickel-zirconium intermetallic compounds  
by Robert Smith Nicholson

A thesis submitted in partial fulfillment of the requirements for the degree of Master of Science in Chemical Engineering  
Montana State University  
© Copyright by Robert Smith Nicholson (1991)

Abstract:

The surface oxide strata that form on nickel-zirconium intermetallic compounds during exposure to air at elevated temperatures were analyzed with dynamic secondary ion mass spectrometry (SIMS). Polycrystalline samples of pure Ni, pure Zr, and the intermetallic compounds Zr<sub>2</sub>Ni, ZrNi, ZrNi<sub>3</sub>, and ZrNi<sub>5</sub> were cleaned, oxidized in air, and then analyzed. Each sample was analyzed after oxidation in air at atmospheric pressure under each of three time-temperature conditions: 300°C for 1 hour, 400°C for 1/2 hour, and 400°C for 1 hour. Dynamic SIMS depth profiling was performed at ultra high vacuum conditions with a 2.0 KeV, .3 microamp, Ar<sup>+</sup> primary ion beam rastered over an approximately 4mm by 4mm area. The signal intensities of four secondary ions, Ni<sup>+</sup>, NiO<sup>+</sup>, Zr<sup>+</sup>, and ZrO<sup>+</sup> were monitored during depth profiling of the surface oxide strata. During steady state sputtering secondary ion signal intensities were monitored while scanning the mass to charge ratio broadscan spectrum from a m/e of 50 to a m/e of 120.

The NiO<sup>+</sup> secondary ion was not detected during analysis of any sample. Experimental observations provide a sound basis for the conclusion that the probability for forming a ZrO<sup>+</sup> secondary ion is greater for oxygen which is a component in the ZrO<sub>2</sub> phase. This study reinforces the conclusions made by others that oxidation of nickel-zirconium intermetallic compounds in air or oxygen at 400°C results in the formation of a surface oxide stratum enriched at the surface in nickel relative to zirconium and indicates that the same phenomenon occurs at 300°C. The signal intensity of the Ni<sup>+</sup> ion during sputtering of NiO is substantially less than the signal intensity of the Zr<sup>+</sup> secondary ion while sputtering ZrO<sub>2</sub>. The Ni<sup>+</sup> secondary ion yield is greater during steady state sputtering of ZrNi, ZrNi<sub>3</sub>, and ZrNi<sub>5</sub> than during the steady state sputtering of pure nickel. For the intermetallic compounds the surface oxide thickness increased with increasing oxidation temperature, time of oxidation, and bulk nickel concentration.

DYNAMIC SECONDARY ION MASS SPECTROMETRY STUDY OF  
SURFACE OXIDE LAYERS OF NICKEL-ZIRCONIUM  
INTERMETALLIC COMPOUNDS

by

Robert Smith Nicholson

A thesis submitted in partial fulfillment  
of the requirements for the degree

of

Master of Science

in

Chemical Engineering

MONTANA STATE UNIVERSITY  
Bozeman, Montana

December 1991

N378  
N526

APPROVAL

of a thesis submitted by

Robert Smith Nicholson

This thesis has been read by each member of the thesis committee and has been found to be satisfactory regarding content, English usage, format, citations, bibliographic style, and consistency, and is ready for submission to the College of Graduate Studies.

12/5/91  
Date

Max C. Deibel  
Chairperson, Graduate Committee

Approved for the Major Department

12/5/91  
Date

John T. Sears  
Head, Major Department

Approved for the College of Graduate Studies

12/19/91  
Date

Henry L. Parsons  
Graduate Dean

## STATEMENT OF PERMISSION TO USE

In presenting this thesis in partial fulfillment of the requirements for a master's degree at Montana State University, I agree that the Library shall make it available to borrowers under rules of the Library. Brief quotations from this thesis are allowable without special permission, provided that accurate acknowledgment of source is made.

Permission for extensive quotations from or reproduction of this thesis may be granted by my major professor, or in his absence, by the Dean of Libraries when, in the opinion of either, the proposed use of the material is for scholarly purposes. Any copying or use of the material in this thesis for financial gain shall not be allowed without my written permission.

Signature

Robert Neuhals

Date

11/30/91

## TABLE OF CONTENTS

	<u>Page</u>
INTRODUCTION . . . . .	1
BACKGROUND . . . . .	3
Zirconium . . . . .	3
Nickel . . . . .	4
The Nickel-Zirconium System . . . . .	5
Intermetallic Compounds . . . . .	6
Formation of Surface Oxide Scales . . . . .	6
Diffusion in Oxides . . . . .	8
Wagner Oxidation Theory in Pure Metals . . . . .	12
Oxidation Theory for Binary Metal Alloys . . . . .	16
Formation of Porous Oxide Scales . . . . .	19
The Dynamic SIMS Analytical Technique . . . . .	21
PRIOR STUDIES OF THE SURFACE OXIDATION OF NICKEL- ZIRCONIUM INTERMETALLIC COMPOUNDS AND ALLOYS . . . . .	27
OBJECTIVES . . . . .	30
EXPERIMENTAL . . . . .	31
Sample Preparation . . . . .	31
Surface Preparation . . . . .	31
Oxidation of Samples . . . . .	32
Surface Analysis . . . . .	33
RESULTS . . . . .	43
Mass Spectra of Sputter Cleaned Surfaces . . . . .	43
Under-Representation of Nickel in Monitored Secondary Ion Yield During Steady State Sputtering . . . . .	47
Secondary Ion Yield Profiles of Oxidized Samples . . . . .	48
Derived Quantity Profiles . . . . .	52
Estimate of Relative Elemental Abundancies in Surface Strata . . . . .	66

## TABLE OF CONTENTS—Continued

	<u>Page</u>
INTERPRETATION . . . . .	72
Reproducibility . . . . .	72
Under-Representation of Oxygenated Secondary Ions in Monitored Secondary Ion Yield Profiles . . . . .	73
Surface Oxide Thickness . . . . .	74
Under-Representation of Nickel in Monitored Secondary Ion Yields . . . . .	75
Surface Enrichment of Nickel During Oxidation . .	77
Relative Abundancies of Nickel and Zirconium in the Surface Strata After Oxidation. . . . .	78
CONCLUSIONS. . . . .	81
Absence of NiO <sup>+</sup> From Secondary Ion Yield. . . . .	81
Ionization Probability of ZrO <sup>+</sup> Secondary Ion. . .	82
Surface Enrichment of Nickel Caused by Surface Oxidation. . . . .	82
The Relative Probability of Forming Ni <sup>+</sup> and Zr <sup>+</sup> Secondary Ions . . . . .	83
Ni <sup>+</sup> Secondary Ion Yield Enhanced by Zr. . . . .	84
Oxide Layer Thickness Dependence on Bulk Composition and Oxidation Conditions . . . . .	85
RECOMMENDATIONS. . . . .	86
Scanning a Wider Mass Number Range. . . . .	86
Post Ionization of Sputtered Neutral Particles. .	87
REFERENCES CITED . . . . .	88
APPENDIX . . . . .	92
Secondary Ion Yield Profiles of Oxidized Samples . . . . .	92

## LIST OF TABLES

Table		<u>Page</u>
1	Relative Natural Abundance of Nickel, Zirconium, and Oxygen Isotopes. . . . .	38
2	Aperture Setting Schedule During Gating Experiment. . . . .	38
3	Count Rates of Ni <sup>58+</sup> , Zr <sup>90+</sup> , and ZrO <sup>106+</sup> Secondary Ions During Steady State Sputtering .	47
4	Factor by Which Nickel Is Under-Represented In Monitored Secondary Ion Yield, K . . . . .	48
5	Estimated Sputter Times Required for Signal Intensities to Reach 90% of Steady State Values During Depth Profiling. . . . .	51
6	R <sub>O/T</sub> Values at the Onset of Sputtering and During Steady State Sputtering. . . . .	59
7	R <sub>Ni/T</sub> Values at the Onset of Sputtering and During Steady State Sputtering. . . . .	65

## LIST OF FIGURES

Figure	<u>Page</u>
1 Partial phase diagram for the nickel-zirconium system. . . . .	7
2 Concentration gradients and reaction pathways for (a) oxide scales containing mostly metal ion vacancies, and for (b) oxide scales containing mostly oxygen ion vacancies . . . . .	15
3 Diagram illustrating (a) the clean surface of the hypothetical intermetallic compound $A_U B_V$ , and (b) the preferential surface oxidation of component A during exposure to oxygen gas . . . .	18
4 Several phenomena that may occur simultaneously during the surface oxidation of the hypothetical intermetallic compound $A_U B_V$ on which forms a composite oxide layer which consists of $A_W O_x$ and $B_Y O_z$ oxide phases . . . . .	20
5 Gating of mass spectrometer output signal for a hypothetical sputter crater . . . . .	24
6 Dynamic SIMS analytical equipment . . . . .	34
7 Count rate changes of selected mass to charge ratios during crater analysis. Aperture setting was varied with time according to the schedule in Table 1. (No $m/e = 74$ signal was observed.) .	39
8 The ratios $R_{58/90}$ , $R_{106/90}$ , and $R_{58/106}$ versus time during crater analysis. Aperture setting varies with time according to the schedule presented in Table 2. . . . .	40
9 Mass spectra generated during broadscan SIMS analysis of sputter cleaned surfaces. Two spectra (solid and dashed lines) are shown for each sample to indicate reproducibility . . . . .	44



## LIST OF FIGURES—Continued

Figure	Page	
10	Broadscan mass spectra for sputter cleaned $ZrNi_3$ . Two spectra (solid and dashed lines) are shown to indicate reproducibility . . . . .	45
11	Signal intensity for the secondary ions, $Ni^{58+}$ , $NiO^{74+}$ , $Zr^{90+}$ , and $ZrO^{106+}$ , versus sputter time during the dynamic SIMS depth profiling of $ZrNi_5$ sample oxidized for one hour at $400^\circ C$ . . .	49
12	Derived quantity ratios, $R_{O/T}$ and $R_{Ni/T}$ , versus sputter time for the data collected during the dynamic SIMS analysis of each of two runs on a $ZrNi_5$ sample oxidized for one hour at $400^\circ C$ . . .	53
13	The ratio, $R_{O/T}$ , versus sputter time for pure Zr samples. . . . .	54
14	The ratio, $R_{O/T}$ , versus sputter time for $Zr_2Ni$ samples . . . . .	55
15	The ratio, $R_{O/T}$ , versus sputter time for ZrNi samples . . . . .	56
16	The ratio, $R_{O/T}$ , versus sputter time for $ZrNi_3$ samples (separate curves are for duplicate runs). . . . .	57
17	The ratio, $R_{O/T}$ , versus sputter time for $ZrNi_5$ samples (separate curves are for duplicate runs). . . . .	58
18	The ratio, $R_{Ni/T}$ , versus sputter time for $Zr_2Ni$ samples . . . . .	61
19	The ratio, $R_{Ni/T}$ , versus sputter time for ZrNi samples . . . . .	62
20	The ratio, $R_{Ni/T}$ , versus sputter time for $ZrNi_3$ samples (separate curves are for duplicate runs). . . . .	63
21	The ratio, $R_{Ni/T}$ , versus sputter time for $ZrNi_5$ samples (separate curves are for duplicate runs). . . . .	64
22	$C_{Ni/T}$ and $C_{Zr/T}$ versus sputter time for analysis of $Zr_2Ni$ for each oxidation condition . . . . .	67
23	$C_{Ni/T}$ and $C_{Zr/T}$ versus sputter time for analysis of ZrNi for each oxidation condition. . . . .	68

## LIST OF FIGURES—Continued

Figure	<u>Page</u>
24	$C_{Ni/T}$ and $C_{Zr/T}$ versus sputter time for analysis of $ZrNi_3$ for each oxidation condition (separate curves are for duplicate runs). . . . . 69
25	$C_{Ni/T}$ and $C_{Zr/T}$ versus sputter time for analysis of $ZrNi_5$ for each oxidation condition (separate curves are for duplicate runs). . . . . 70
26	Signal intensity of the secondary ions, $Ni^{58+}$ and $NiO^{74+}$ , versus sputter time during the dynamic SIMS depth profiling of a pure Ni sample oxidized for 1 hour at 300°C . . . . . 93
27	Signal intensity of the secondary ions, $Ni^{58+}$ and $NiO^{74+}$ , versus sputter time during the dynamic SIMS depth profiling of a pure Ni sample oxidized for 1 hour at 300°C . . . . . 94
28	Signal intensity of the secondary ions, $Ni^{58+}$ and $NiO^{74+}$ , versus sputter time during the dynamic SIMS depth profiling of an Ni sample oxidized for 1/2 hour at 400°C. . . . . 95
29	Signal intensity of the secondary ions, $Ni^{58+}$ and $NiO^{74+}$ , versus sputter time during the dynamic SIMS depth profiling of an Ni sample oxidized for 1 hour at 400°C. . . . . 96
30	Signal intensity of the secondary ions, $Ni^{58+}$ and $NiO^{74+}$ , versus sputter time during the dynamic SIMS depth profiling of an Ni sample oxidized for 1 hour at 400°C. . . . . 97
31	Signal intensity of the secondary ions, $Zr^{90+}$ and $ZrO^{106+}$ , versus sputter time during the dynamic SIMS depth profiling of a Zr sample oxidized for 1 hour at 300°C. . . . . 98
32	Signal intensity of the secondary ions, $Zr^{90+}$ and $ZrO^{106+}$ , versus sputter time during the dynamic SIMS depth profiling of a Zr sample oxidized for 1/2 hour at 400°C. . . . . 99
33	Signal intensity of the secondary ions, $Zr^{90+}$ and $ZrO^{106+}$ , versus sputter time during the dynamic SIMS depth profiling of a Zr sample oxidized for 1 hour at 400°C. . . . . 100

## LIST OF FIGURES--Continued

Figure	Page	
34	Signal intensity of the secondary ions, $\text{Ni}^{58+}$ , $\text{NiO}^{74+}$ , $\text{Zr}^{90+}$ , and $\text{ZrO}^{106+}$ , versus sputter time during the dynamic SIMS depth profiling of a $\text{Zr}_2\text{Ni}$ sample oxidized for 1 hour at $300^\circ\text{C}$ . . . . .	101
35	Signal intensity of the secondary ions, $\text{Ni}^{58+}$ , $\text{NiO}^{74+}$ , $\text{Zr}^{90+}$ , and $\text{ZrO}^{106+}$ , versus sputter time during the dynamic SIMS depth profiling of a $\text{Zr}_2\text{Ni}$ sample oxidized for 1/2 hour at $400^\circ\text{C}$ . . . . .	102
36	Signal intensity of the secondary ions, $\text{Ni}^{58+}$ , $\text{NiO}^{74+}$ , $\text{Zr}^{90+}$ , and $\text{ZrO}^{106+}$ , versus sputter time during the dynamic SIMS depth profiling of a $\text{Zr}_2\text{Ni}$ sample oxidized for 1 hour at $400^\circ\text{C}$ . . . . .	103
37	Signal intensity of the secondary ions, $\text{Ni}^{58+}$ , $\text{NiO}^{74+}$ , $\text{Zr}^{90+}$ , and $\text{ZrO}^{106+}$ , versus sputter time during the dynamic SIMS depth profiling of a $\text{ZrNi}$ sample oxidized for 1 hour at $300^\circ\text{C}$ . . . . .	104
38	Signal intensity of the secondary ions, $\text{Ni}^{58+}$ , $\text{NiO}^{74+}$ , $\text{Zr}^{90+}$ , and $\text{ZrO}^{106+}$ , versus sputter time during the dynamic SIMS depth profiling of a $\text{ZrNi}$ sample oxidized for 1/2 hour at $400^\circ\text{C}$ . . . . .	105
39	Signal intensity of the secondary ions, $\text{Ni}^{58+}$ , $\text{NiO}^{74+}$ , $\text{Zr}^{90+}$ , and $\text{ZrO}^{106+}$ , versus sputter time during the dynamic SIMS depth profiling of a $\text{ZrNi}$ sample oxidized for 1 hour at $400^\circ\text{C}$ . . . . .	106
40	Signal intensity of the secondary ions, $\text{Ni}^{58+}$ , $\text{NiO}^{74+}$ , $\text{Zr}^{90+}$ , and $\text{ZrO}^{106+}$ , versus sputter time during the dynamic SIMS depth profiling of a $\text{ZrNi}_3$ sample oxidized for 1 hour at $300^\circ\text{C}$ . . . . .	107
41	Signal intensity of the secondary ions, $\text{Ni}^{58+}$ , $\text{NiO}^{74+}$ , $\text{Zr}^{90+}$ , and $\text{ZrO}^{106+}$ , versus sputter time during the dynamic SIMS depth profiling of a $\text{ZrNi}_3$ sample oxidized for 1/2 hour at $400^\circ\text{C}$ . . . . .	108
42	Signal intensity of the secondary ions, $\text{Ni}^{58+}$ , $\text{NiO}^{74+}$ , $\text{Zr}^{90+}$ , and $\text{ZrO}^{106+}$ , versus sputter time during the dynamic SIMS depth profiling of a $\text{ZrNi}_3$ sample oxidized for 1/2 hour at $400^\circ\text{C}$ . . . . .	109

## LIST OF FIGURES—Continued

Figure		Page
43	Signal intensity of the secondary ions, $\text{Ni}^{58+}$ , $\text{NiO}^{74+}$ , $\text{Zr}^{90+}$ , and $\text{ZrO}^{106+}$ , versus sputter time during the dynamic SIMS depth profiling of a $\text{ZrNi}_3$ sample oxidized for 1/2 hour at $400^\circ\text{C}$ . . .	110
44	Signal intensity of the secondary ions, $\text{Ni}^{58+}$ , $\text{NiO}^{74+}$ , $\text{Zr}^{90+}$ , and $\text{ZrO}^{106+}$ , versus sputter time during the dynamic SIMS depth profiling of a $\text{ZrNi}_3$ sample oxidized for 1 hour at $400^\circ\text{C}$ . . . .	111
45	Signal intensity of the secondary ions, $\text{Ni}^{58+}$ , $\text{NiO}^{74+}$ , $\text{Zr}^{90+}$ , and $\text{ZrO}^{106+}$ , versus sputter time during the dynamic SIMS depth profiling of a $\text{ZrNi}_3$ sample oxidized for 1 hour at $400^\circ\text{C}$ . . . .	112
46	Signal intensity of the secondary ions, $\text{Ni}^{58+}$ , $\text{NiO}^{74+}$ , $\text{Zr}^{90+}$ , and $\text{ZrO}^{106+}$ , versus sputter time during the dynamic SIMS depth profiling of a $\text{ZrNi}_5$ sample oxidized for 1 hour at $300^\circ\text{C}$ . . . .	113
47	Signal intensity of the secondary ions, $\text{Ni}^{58+}$ , $\text{NiO}^{74+}$ , $\text{Zr}^{90+}$ , and $\text{ZrO}^{106+}$ , versus sputter time during the dynamic SIMS depth profiling of a $\text{ZrNi}_5$ sample oxidized for 1/2 hour at $400^\circ\text{C}$ . . .	114
48	Signal intensity of the secondary ions, $\text{Ni}^{58+}$ , $\text{NiO}^{74+}$ , $\text{Zr}^{90+}$ , and $\text{ZrO}^{106+}$ , versus sputter time during the dynamic SIMS depth profiling of a $\text{ZrNi}_5$ sample oxidized for 1 hour at $400^\circ\text{C}$ . . . .	115
49	Signal intensity of the secondary ions, $\text{Ni}^{58+}$ , $\text{NiO}^{74+}$ , $\text{Zr}^{90+}$ , and $\text{ZrO}^{106+}$ , versus sputter time during the dynamic SIMS depth profiling of a $\text{ZrNi}_5$ sample oxidized for 1 hour at $400^\circ\text{C}$ . . . .	116

## ABSTRACT

The surface oxide strata that form on nickel-zirconium intermetallic compounds during exposure to air at elevated temperatures were analyzed with dynamic secondary ion mass spectrometry (SIMS). Polycrystalline samples of pure Ni, pure Zr, and the intermetallic compounds  $Zr_2Ni$ ,  $ZrNi$ ,  $ZrNi_3$ , and  $ZrNi_5$  were cleaned, oxidized in air, and then analyzed. Each sample was analyzed after oxidation in air at atmospheric pressure under each of three time-temperature conditions: 300°C for 1 hour, 400°C for 1/2 hour, and 400°C for 1 hour. Dynamic SIMS depth profiling was performed at ultra high vacuum conditions with a 2.0 KeV, .3 microamp,  $Ar^+$  primary ion beam rastered over an approximately 4mm by 4mm area. The signal intensities of four secondary ions,  $Ni^+$ ,  $NiO^+$ ,  $Zr^+$ , and  $ZrO^+$  were monitored during depth profiling of the surface oxide strata. During steady state sputtering secondary ion signal intensities were monitored while scanning the mass to charge ratio broadscan spectrum from a m/e of 50 to a m/e of 120.

The  $NiO^+$  secondary ion was not detected during analysis of any sample. Experimental observations provide a sound basis for the conclusion that the probability for forming a  $ZrO^+$  secondary ion is greater for oxygen which is a component in the  $ZrO_2$  phase. This study reinforces the conclusions made by others that oxidation of nickel-zirconium intermetallic compounds in air or oxygen at 400°C results in the formation of a surface oxide stratum enriched at the surface in nickel relative to zirconium and indicates that the same phenomenon occurs at 300°C. The signal intensity of the  $Ni^+$  ion during sputtering of NiO is substantially less than the signal intensity of the  $Zr^+$  secondary ion while sputtering  $ZrO_2$ . The  $Ni^+$  secondary ion yield is greater during steady state sputtering of  $ZrNi$ ,  $ZrNi_3$ , and  $ZrNi_5$  than during the steady state sputtering of pure nickel. For the intermetallic compounds the surface oxide thickness increased with increasing oxidation temperature, time of oxidation, and bulk nickel concentration.

## INTRODUCTION

The objective of this research is to analyze with dynamic secondary ion mass spectrometry (SIMS) the surface oxide strata that form on nickel-zirconium intermetallic compounds during exposure to air at elevated temperatures. Results of previous investigations of this system by other analytical methods provide information useful for interpretation of secondary ion yield profiles [1,2,3,4,5].

The distribution of a metallic component between the bulk substance and its outer surfaces often plays a critical role in determining its utility for given applications. The composition and structure of the material contained in the surface region is commonly quite different from that of the bulk. Many metals and alloys exhibit a fully developed surface stratum which is only a few atomic layers thick. The primary importance of surface layers to the materials scientist is their influence on interactions between the bulk substance and the outside environment [6,7,8,9].

The formation of surface strata on clean metallic surfaces during oxidation is the result of interactions with the surroundings. There are several driving forces and hindrances for the processes taking place during the development of surface strata. Reaction kinetics influence

oxidation rates. Mass transport considerations govern diffusion of various species. The equilibrium state of the system is analyzed through thermodynamics. The interplay between these simultaneous processes, however, is often involved, resulting in complex reaction pathways [10,11,12].

Although the desire for further investigation of the formation and structure of surface strata on metals might be rooted in the curiosity of the materials scientist, a justification arises from the tremendous industrial importance of the stability of metals. There exists a definite and well-known need for metallic materials that are technically superior to those which are currently available. The cost to American industry resulting from corrosion of metallic components is on the order of billions of dollars annually [8]. The development and widespread availability of capable analytical methods for the characterization of surface strata on an atomic scale has been relatively recent. These developments combined with rapid gains in technology in other fields have increased the importance of further investigations.

## BACKGROUND

### Zirconium

Zirconium is used extensively in the nuclear power industry as a major constituent of various fuel cladding alloys that separate the fuel from coolant water in atomic reactors. The most widely used is Zircaloy-2. It consists of zirconium and tin, plus minor additions of chromium, iron, and nickel for better corrosion resistance. Zirconium has a low capture cross section for neutrons. This means that neutrons pass freely through bulk zirconium without appreciable energy loss and corresponding temperature rise of the cladding material. Zirconium based fuel cladding alloys are resistant to the corrosive environment in atomic reactors. An average size nuclear power generating facility may use half a million feet of zirconium alloy tubing. About 90% of zirconium metal production is used in nuclear applications [13,14,15].

Zirconium is well suited for many applications outside the nuclear power industry. It is especially resistant to corrosion by sea water and many common acids and bases. It is used extensively in the chemical industry where corrosive agents are dealt with. Two examples of components made of zirconium or zirconium based alloys for which oxidation



resistance is important are explosive primers and lamp filaments [9,13].

The corrosion resistance of zirconium based alloy components is due to the formation of a cohesive-inert surface oxide layer. Zirconium is actually very reactive with oxygen. Finely divided Zr particles ignite spontaneously in air at elevated temperatures [13]. In many environments, however, the rapid interaction between a clean zirconium surface and oxygen results in the formation of a cohesive and impermeable surface oxide layer that prevents further oxidation of the bulk metal. The protective oxide layer that forms on clean zirconium surfaces in air at room temperature has been reported to consist of approximately 3 or 4 molecular layers of sub-stoichiometric  $ZrO_2$  [15,16].

#### Nickel

The properties and availability of metallic nickel make it well suited for a variety of applications. It is hard, malleable, and ductile, and takes on a high electricity. It is available in many mill forms as well as castings. Nickel and iron probably make up most of the core of the earth [17,18].

Nickel performs very well in many corrosive environments. Components made of nickel maintain their integrity in sea water. Nickel is resistant to corrosion by alkalies and is widely used for their handling; particularly

in concentrating, shipping and storing high purity caustic soda. Steel, iron, bronze, copper, and many other pure metals and alloys are plated with nickel for corrosion resistance in various environments [18,19].

Nickel is a minor or major constituent of many important alloys. Stainless steel, nickel steel, Invar, Monel, Hastelloy, Constantan, Nichrome, Chromel, and Permalloy are some of the more common alloys that contain nickel. Chromel and Nichrome, both of which are composed of nickel, iron, and chromium, are oxidation resistant in air at high temperatures and have relatively high electrical resistances. For these reasons they are used for heating wires in appliances such as toasters and blow dryers. Nickel steel is extremely hard and used for armor plate and bullet proof vaults. The monels which consist primarily of nickel and copper are used in systems which convert sea water to fresh water, among other applications [17,18,19].

#### The Nickel-Zirconium System

The nickel-zirconium alloy system was chosen for a case study of oxide scales formed during exposure to air at elevated temperatures in this research program. Both components exhibit very good oxidation resistance under a wide variety of conditions in their pure form and when alloyed with many other metals. Alloys having both nickel and zirconium components play a vital role in many

industrial processes requiring metallic components with high resistance to oxidation and good mechanical properties. Prime examples are the previously described zircalloys.

Phase equilibrium data for the nickel-zirconium system is available in the form of a comprehensive phase diagram, Figure 1 [20]. Along with the terminal solid solutions this system contains eight intermetallic phases. None of these ten phases exhibits very extensive intersolubility [20]. Pure Nickel, pure zirconium, and the intermetallic compounds,  $Zr_2Ni$ ,  $ZrNi$ ,  $ZrNi_3$ , and  $ZrNi_5$ , were selected for this research.

#### Intermetallic Compounds

Although the majority of industrially important alloys are polyphase composites, single phase metal samples are better for many oxide scale studies. Their use circumvents the problem of interpreting experimental data obtained from two or more exposed surface phases simultaneously [21]. Almost pure intermetallic compound samples are readily produced by heating and melting stoichiometric mixtures of the pure metals [1].

#### Formation of Surface Oxide Scales

A surface oxide layer forms on most metals during oxidation in air [6]. Thermodynamically the free energies of oxides are generally lower than that of the reduced metal

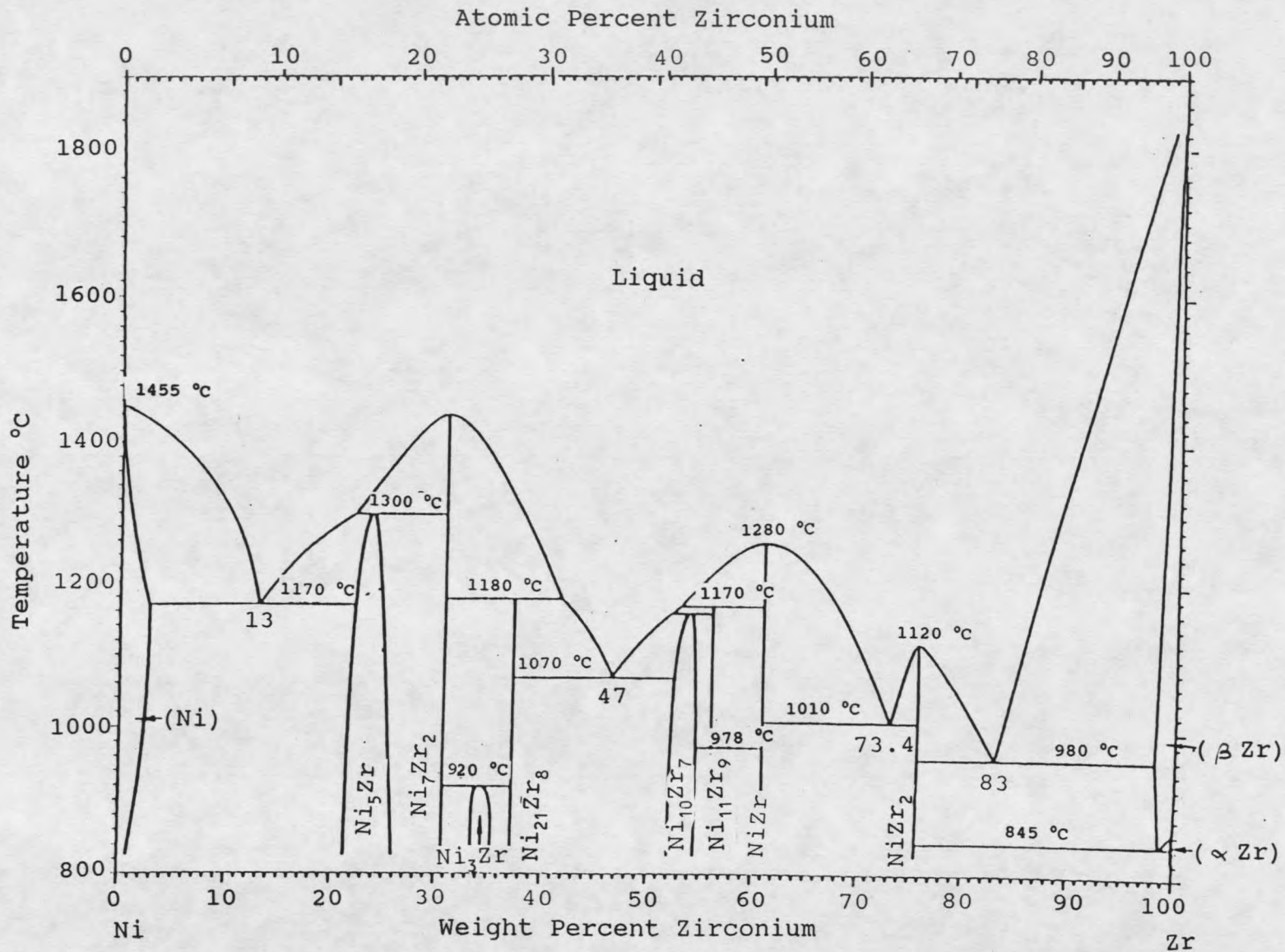


Figure 1. Partial phase diagram for the nickel-zirconium system [20]

in contact with oxygen gas. Kinetically the activation energy for the reaction is probably not insurmountable, at least at elevated temperatures. Also the reduced metal and oxygen gas are in direct contact during the initial stages of oxidation [6,10].

The mechanism for metal oxidation is dependent on the nature of the oxide layer that forms. Oxide layers may be either porous or compact. Improved oxidation resistance in metals and alloys is usually realized through enhancing the protective properties of the surface oxide layer [6].

Compact oxide layers offer the best protection against high temperature oxidation because they form a nonporous barrier between the reduced metal and oxygen in the gas. For compact oxide layers the rate of the oxidation will be limited by the solid state diffusion of reactants through the oxide layer. As the oxide layer thickness grows, the diffusion distance increases, causing the oxidation rate to decrease [6].

#### Diffusion in Oxides

Solid state diffusion of oxygen and/or metal ions through a surface oxide layer is facilitated by the presence of mobile imperfections or defects in the lattice structure. These point defects are always present in crystalline structures at temperatures greater than 0 K. The creation of point defects in a crystal increases both the internal energy and the entropy of the system. The equilibrium

concentration will be reached when the free energy of the system is at a minimum. Many types of defects are possible but one type of defect structure commonly dominates in a particular solid under given conditions [22,23].

Relative concentrations of different types of defects are highly temperature dependent. Thus, point defects with large positive enthalpies of formation which are not important at lower temperature may become important at high temperatures [24].

Metal and oxygen ion vacancies are the two most important types of point defects for lattice diffusion of metal and oxygen ions in oxides. A metal ion vacancy is a vacant cation lattice site that would be occupied by a metal ion in the absence of a defect at that location. An oxygen ion vacancy is an unoccupied anion lattice site which would normally contain an oxygen ion [22,23,24].

The equilibrium concentration of defects at the surface of an oxide is dependent on the ambient oxygen partial pressure. The equilibrium concentration of metal ion vacancies will increase with increased oxygen partial pressure. The equilibrium concentration of oxygen ion vacancies will decrease with increased oxygen partial pressure [6].

Interstitial atoms are another type of lattice defect. Interstitial atoms occupy regions in the lattice structure called interstitial sites which would otherwise be vacant.

Interstitial atoms that are relatively small compared to the normal lattice atoms distort the lattice much less than ones that are nearly the same size or larger than the normal lattice atoms [25,26].

Charge neutrality is maintained in a lattice in spite of the presence of point defects. Charge neutrality can be realized with either the presence of nearby oppositely charged lattice defects or the presence of electron delocalized valence defects which may be conveniently considered to be free electrons and/or electron holes [27,28].

Movement of ions within an oxide lattice structure takes place when ions leave normal lattice sites to fill adjacent ion vacancies. Diffusion which is based on this fundamental movement is said to proceed by a vacancy mechanism. A given net flux of ions will constitute an equal net flux of vacancies along with any associated electron defects in the opposite direction [22,23].

Diffusion is said to occur by an interstitial mechanism when an interstitial atom moves from the site that it occupies to an adjacent interstitial site. This diffusion mechanism may be dominant in lattices where the diffusing interstitial atoms are relatively small compared to the normal lattice atoms. The interstitial mechanism is thought to operate in alloys where solute atoms normally occupy interstitial positions. For metal oxide lattice structures,

however, diffusion by the interstitial mechanism is generally unimportant and lattice diffusion occurs by the vacancy mechanism almost exclusively. The reason is that oxygen and metal ions are generally large compared to the interstitial sites in oxides and their movement by an interstitial mechanism would require distortions of too great of magnitude to occur significantly [25,26].

Fick's law is valid for lattice diffusion. The following equation expresses Fick's law as it applies to solid state diffusion by a vacancy mechanism.

$$(1) \quad J = - D \frac{d[V]}{dx}$$

Where:

- J ≡ The diffusive flux
- D ≡ The diffusion coefficient
- [V] ≡ The vacancy concentration
- x ≡ Position

The diffusion coefficient is related to temperature and lattice parameters. An atom passes through a high energy, intermediate position when it moves from a normal lattice site to a vacancy or from one interstitial site to an adjacent one. The energy requirement or barrier is called the activation energy for the process. Only a certain fraction of the atoms that are in a position to make such a move have sufficient energy. Since that fraction increases exponentially with temperature, diffusion is a thermally activated process. The temperature and activation energy



dependence of the diffusion coefficient can often be expressed by the following Arrhenius relationship [29].

$$(2) \quad D \propto \text{EXP}[E_A/RT]$$

Where:

$E_A$	$\equiv$	Activation energy for the fundamental atomic movement of diffusion
$R$	$\equiv$	Ideal gas constant
$T$	$\equiv$	Absolute temperature

Grain boundaries, and dislocations provide other avenues for diffusion. Because diffusion along these paths is generally more rapid than for lattice diffusion these are termed high diffusivity or low resistance paths. Although grain boundary and dislocation diffusion are likely to be more rapid, these paths generally occupy only a small portion of the area normal to the diffusive flux. Grain boundary diffusion may be particularly significant at low temperatures where the fraction of atoms that acquire the activation energy for lattice diffusion is negligible. It is generally difficult to experimentally verify or estimate quantitatively the relative importance of grain boundary diffusion and lattice diffusion [30,31,32].

#### Wagner Oxidation Theory in Pure Metals

The well known and widely applied oxidation theory formulated by Carl Wagner is the most useful for understanding high temperature oxidation of pure metals [6,11,12]. The essential features of surface oxidation are addressed and related by the Wagner theory. This provides

an excellent theoretical basis for understanding the surface oxidation of metals.

Wagner oxidation theory applies to compact surface oxide layers and is based on several simplifying assumptions. It assumes that diffusion of reactants, the metal ions, oxygen ions, or both, through the developing oxide layer is the rate limiting step. Ions and electrons, or conversely vacancies and electron holes, are assumed to migrate independently of one another. Reactions occurring at the metal/oxide and oxide/gas phase boundaries are assumed to proceed rapidly relative to diffusion in the oxide layer. For this reason, thermodynamic equilibrium is assumed to exist at both the oxide/gas and oxide/metal phase boundaries [6].

In the Wagner oxidation model, concentration gradients are established in developing oxide scales since a different thermodynamic equilibrium state is maintained at the two phase boundaries. The concentration of metal and oxygen ion vacancies at the metal/oxide interface is related to the equilibrium dissociation pressure of the oxide. At the oxide/gas interface the concentration of metal and oxygen ion vacancies is related to the partial pressure of oxygen in the gas phase. Concentration gradients result in diffusion of one or more species which leads to further reaction and oxide growth. Concentration gradients and resulting reaction paths are illustrated in Figure 2 for the

cases of oxide layers containing mostly metal ion vacancies and for those with mostly oxygen ion vacancies, respectively [6,11,12]. The variables in Figure 2 are defined as follows:

$V_M^{p-}$	represents metal ion vacancies
$V_O^{q+}$	represents oxygen ion vacancies
$e^+$	represents electron holes
$e^-$	represents electrons
[ ]	indicates concentration
M	is the hypothetical metal
$M_qO_p$	is the hypothetical metal oxide
f	is the functional dependence of $V_M^{p-}$ on $P_{O_2}$
g	is the functional dependence of $V_O^{q+}$ on $P_{O_2}$
$P_{O_2}^{(d)}$	$\equiv$ the dissociation pressure of the oxide
$P_{O_2}^{(g)}$	$\equiv$ the ambient oxygen partial pressure
h	$\equiv$ thickness of the oxide layer

Wagner oxidation theory predicts that the growth rate of a compact surface oxide layer decreases with time and increasing oxide layer thickness [6,11,12]. Since interfacial oxidation reactions are assumed to proceed rapidly, the growth rate of the developing scale is proportional to the rate of diffusion of the reacting species. The following expression relates the growth rate of the developing scale,  $dh/dt$ , to thickness,  $h$ , and the concentration profile for oxide scales having mostly metal ion vacancies.

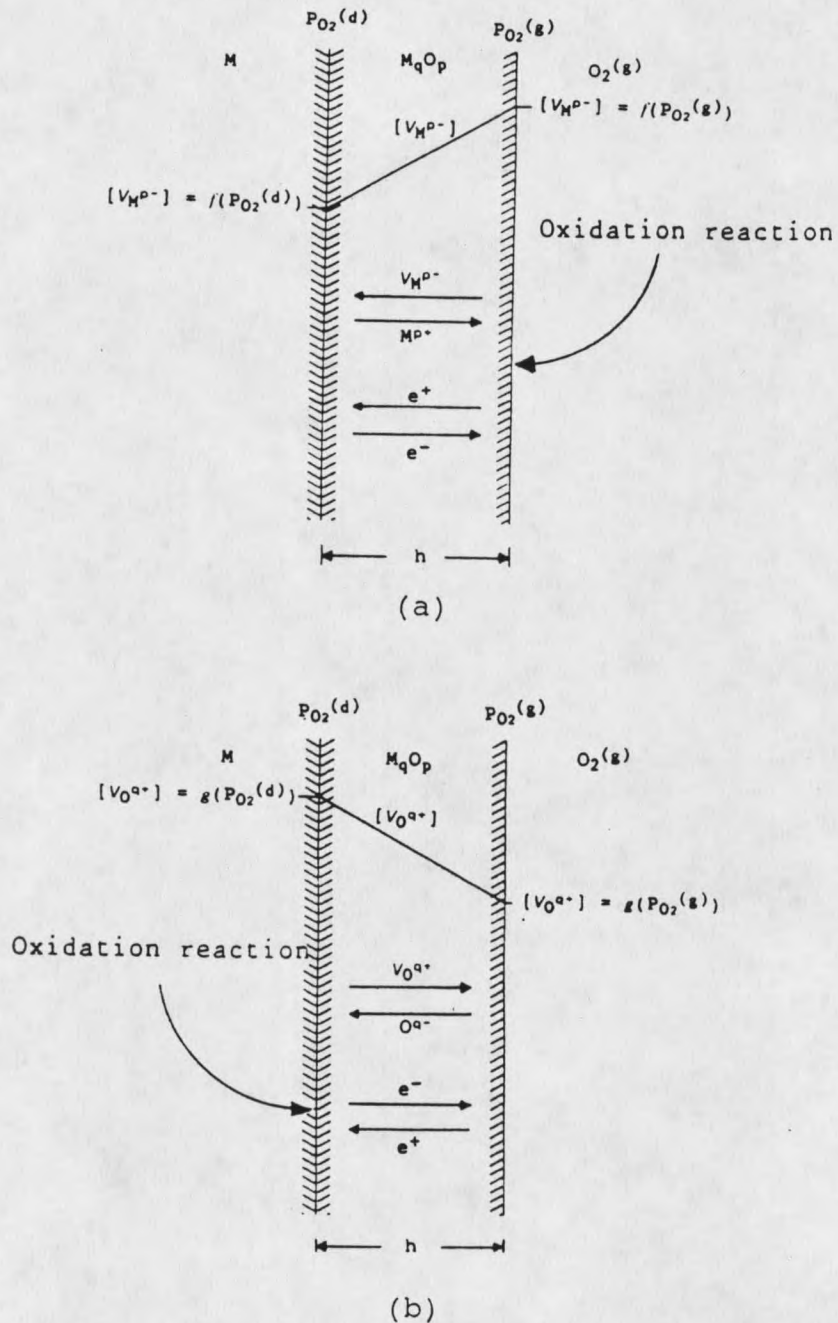


Figure 2. Concentration gradients and reaction pathways for (a) oxide scales containing mostly metal ion vacancies and for (b) oxide scales containing mostly oxygen ion vacancies.

$$(3) \quad dh/dt \propto J = D \frac{([V_M^{P^-}]_{MO/O_2} - [V_M^{P^-}]_{M/MO})}{h}$$

Subscripts, M/MO and MO/O<sub>2</sub>, denote concentration at the metal/oxide and oxide/gas interfaces respectively. The rate of growth of oxide scales having mostly oxygen ion vacancies is related to the concentration profile and thickness by a similar expression.

$$(4) \quad dh/dt \propto J = D \frac{([V_O^{q+}]_{M/MO} - [V_O^{q+}]_{MO/O_2})}{h}$$

Since concentrations of the metal and oxygen ion vacancies are assumed to be fixed at both interfaces the following expression relates dh/dt to scale thickness for both cases.

$$(5) \quad dh/dt \propto 1/h$$

Separating variables and integrating yields the time dependence of h during oxidation.

$$(6) \quad h \propto t_{1/2}$$

Further differentiation yields the time dependence of dh/dt.

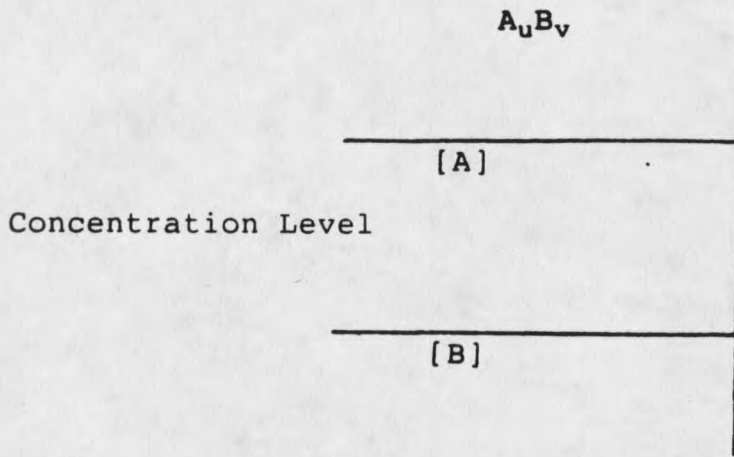
$$(7) \quad dh/dt \propto t_{-1/2}$$

### Oxidation Theory for Binary Metal Alloys

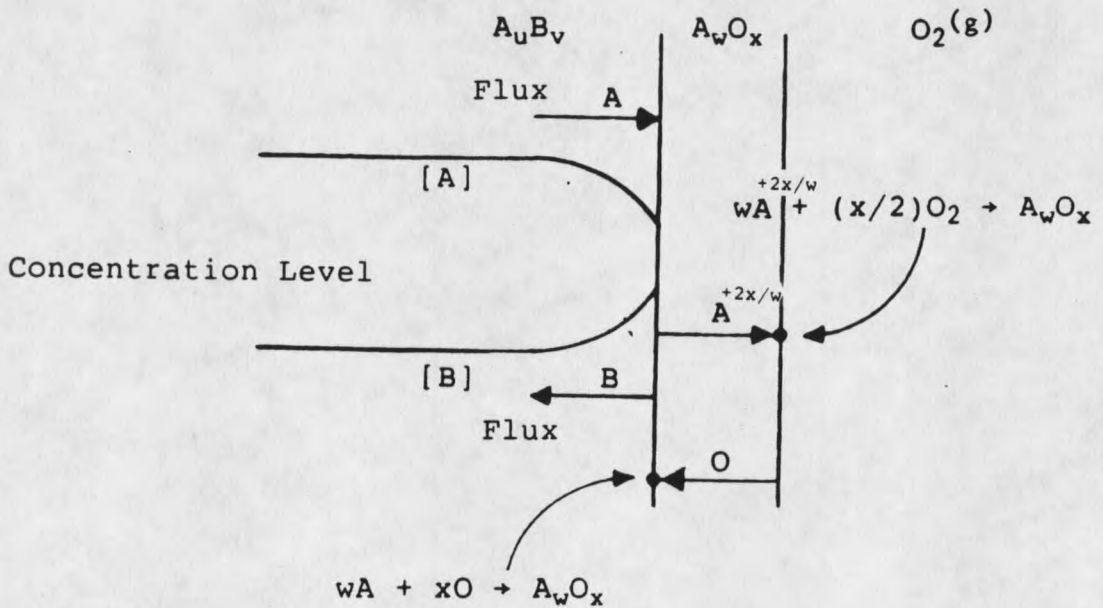
Wagner oxidation theory for metal alloys is inherently more complex than for pure metals. Composite oxide scales which contain two or more mixed oxide phases commonly form

on alloys during high temperature oxidation. Cation displacement reactions may occur at interfaces separating adjacent oxide phases. The metallic components will generally differ in their affinities for oxygen and their mobilities in the oxide phases. The composition of the metal at the metal/oxide interface will change with extent of reaction when one metallic component is preferentially oxidized at the metal/oxide interface or when one metallic component diffuses outward from the metal/oxide interface more rapidly. Concentration gradients in the metal near the metal/oxide interface will develop. Outward diffusion of the depleted species in the metal and inward diffusion of the other will result.

The surface oxidation of a hypothetical intermetallic compound,  $A_uB_v$ , is shown schematically in Figure 3. For the oxidation reaction depicted in Figure 3 it is assumed that component A is being oxidized to form  $A_wO_x$ . Component B is assumed to be neither reacting with oxygen at the metal/oxide interface nor diffusing into the developing  $A_wO_x$  scale. In the metal near the metal/oxide interface the concentration of B relative to A increases with extent of reaction. At some point in time B may start to react with oxygen at the metal/oxide interface or diffuse through the layer of  $A_wO_x$  to react with oxygen at the oxide/gas interface.



(a)



(b)

Figure 3. Diagram illustrating (a) the clean surface of the hypothetical intermetallic compound  $A_uB_v$  and (b) the preferential surface oxidation of component A during exposure to oxygen gas.

Reaction pathways for the surface oxidation of intermetallic compounds that form composite oxides are potentially complicated and difficult to predict. Both the metal ions and oxygen ions might diffuse through the oxide phases. Oxidation could occur at the interface between an oxide phase and the bulk metal, the gas phase, or the other oxide phase. Perhaps a reaction will occur where the cations of one of the metals will displace those of the other metal across the interface between two adjacent oxide phases. Figure 4 illustrates several phenomena that might occur during the surface oxidation of the hypothetical intermetallic compound  $A_uB_v$  which forms a composite surface oxide of  $A_wO_x$  and  $B_yO_z$  phases. Not shown in Figure 4 but a possibility, nonetheless, is the formation of mixed oxide phases,  $A_rB_sO_t$  for example.

#### Formation of Porous Oxide Scales

The preceding discussion has been limited to compact surface oxide layers. Porous oxide scales can form initially or compact scales may later become porous. Void spaces left at the metal/oxide interface by cations diffusing into the oxide phase may act as either a barrier or a low resistance path for further diffusion. Compact oxides may grow to a critical thickness and then rupture from any of the various mechanical stresses that can be present in the surface oxide layer. If the reaction





























































































































































































































